



Synthesis and characterization of 3-methyl-5-oxo-N,1-diphenyl-4,5-dihydro-1-H-pyrazole-4-carbothioamide and its metal complexes

R.M. El-Shazly*

Chemistry Department, Faculty of Science, Mansoura University, Abdel-Salam Aref, Mansoura, Egypt

ARTICLE INFO

Article history:

Received 14 December 2008

Received in revised form 2 June 2009

Accepted 7 June 2009

Keywords:

3-Methyl-5-oxo-N,1-diphenyl-4,5-dihydro-1-H-pyrazole-4-carbothioamide

Complex

Spectra

Thermogravimetry

ABSTRACT

The molecular parameters have been calculated to confirm the geometry of 3-methyl-5-oxo-N,1-diphenyl-4,5-dihydro-1-H-pyrazole-4-carbothioamide, HL. The compound is introduced as a new chelating agent for complexation with Cr(III), Fe(III), Co(II), Ni(II) and Cu(II) ions. The isolated chelates were characterized by partial elemental analyses, magnetic moments, spectra (IR, UV–vis, ESR; ¹H NMR) and thermal studies. The protonation constant of HL (5.04) and the stepwise stability constants of its Co(II), Cu(II), Cr(III) and Fe(III) complexes were calculated. The ligand coordinates as a monobasic bidentate through hydroxo and thiol groups in all complexes except Cr(III) which acts as a monobasic monodentate through the enolized carbonyl oxygen. Cr(III) and Fe(III) complexes measured normal magnetic moments; Cu(II) and Co(II) measured subnormal while Ni(II) complex is diamagnetic. The data confirm a high spin and low spin octahedral structures for the Fe(III) and Co(II) complexes. The ESR spectrum of the Cu(II) complex support the binuclear structure. The molecular parameters have also been calculated for the Cu(II) and Fe(III) complexes. The thermal decomposition stages of the complexes confirm the MS to be the residual part. Also, the thermodynamic and kinetic parameters were calculated for some decomposition steps.

© 2009 Elsevier B.V. All rights reserved.

1. Introduction

Thione compounds and their metal complexes have a noticeable antimicrobial activity and the substituents play an important role in enhancing the activity [1]. The multicoordination centers gave the ability to form stable chelates with the essential metal ions in which the organisms need in their metabolism [2]. Oxygen, nitrogen and sulfur compounds are extensively studied [3–8] which covered different areas including the effect of active donors and electron delocalization in transition metal complexes as well as the antimicrobial activity. Some have been tested as fungicides for textile fabrics. Binuclear complexes of N-benzoyl-N'-(2-hydroxyphenyl)thiocarbamide, with Cu(II), Co(II) and Ni(II) have been synthesized. The ligand acts as a tridentate dibasic donor coordinating through carbonyl oxygen, thiocarbamido sulfur and deprotonated phenolic oxygen to yield the metal complexes in which water is replaceable by pyridine or picolines [9]. The complexes of Cu(II), Co(II), Ni(II), Zn(II), Cd(II) and Pd(II) with 3-(N-phenylthiocarbamyl)pentan-2,4-dione, ethyl- α -(N-phenylthio-carbamyl)cyanoacetate and ethyl- α -(N-phenylthiocarbamyl)acetoacetate were prepared and characterized [10–12].

In continuation, 3-methyl-5-oxo-N,1-diphenyl-4,5-dihydro-1-H-pyrazole-4-carbo-thioamide, (Fig. 1) and their metal complexes have been studied. The geometries of the complexes are characterized by means of spectral, magnetic and thermal measurements.

2. Experimental

2.1. Materials

The metal salts used in this work: CrCl₃·6H₂O, FeCl₃·9H₂O, Ni(OAc)₂·4H₂O, Co(OAc)₂·2H₂O and Cu(OAc)₂·H₂O are of analytical grade and supplied from Aldrich.

3-Methyl-5-oxo-N,1-diphenyl-4,5-dihydro-1-H-pyrazole-4-carbothioamide (IUPAC name, Fig. 1) was prepared similar to that reported earlier [13]. To confirm the purity of the synthesized ligand, its ¹H NMR spectrum (Fig. 2a) in d₆-DMSO is recorded. The peaks observed at 13.052 (s, 1H), [7.877–7.199], 2.782 (s, 3H) and 2.528 (s, 1H) ppm are mainly due to the NH, (phenyl groups), CH₃ and CH protons, respectively. The molecular modeling of HL is shown in Fig. 1S.

2.2. Synthesis of complexes

The complexes were prepared by mixing 0.37 g of the ligand (1 mmol) dissolved in 20 ml EtOH and the required amount of the metal salt (2 mmol) in 30 ml EtOH and heated under reflux

* Tel.: +20 101645967.

E-mail address: raafetmansour9@yahoo.com.

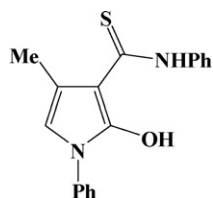


Fig. 1. Formula of HL.

on a water bath for 0.5–1 h. In all preparations, the precipitate was filtered off, washed with ethanol and diethylether and finally dried in a vacuum desiccator. In the preparation of Cu(II) complex, $\text{Cu}(\text{OAc})_2 \cdot \text{H}_2\text{O}$ was dissolved in H_2O –EtOH and the precipitate was washed with water, ethanol and diethylether, respectively.

2.3. Physical measurements

Partial elemental analyses (C, H and N) were performed on a PerkinElmer, Series II CHNS/O 2400 Analyzer at the Microanalytical Unit of Cairo University. Cu(II), Co(II), Ni(II), Fe(III) and Cr(III) analyses were carried out complexometrically. The IR spectra, as KBr discs, were carried out on a Mattson 5000 FTIR Spectrophotometer (400 – 4000 cm^{-1}) at Mansoura University, Egypt. The electronic spectra, as Nujol mull and DMF solution, were recorded on a UV₂ Unicam UV/vis at Mansoura University, Egypt. The magnetic moment values were evaluated at room temperature ($25 \pm 1^\circ\text{C}$) using a Johnson Matthey magnetic susceptibility balance. The thermal studies were carried out on a Shimadzu thermogravimetric analyzer at a heating rate of $10^\circ\text{C min}^{-1}$ under nitrogen gas. The ESR spectrum of Cu(II) was obtained on a Bruker EMX Spectrometer working in the X-band (9.78 GHz) with 100 kHz modulation frequency. The microwave power and the modulation amplitude were set at 1 mW and 4 G, respectively. The low field signal was obtained after four scans with a 10-fold increase in the receiver gain. Powder ESR spectra were obtained in 2 mm quartz capillaries at room temperature ($25 \pm 1^\circ\text{C}$). All molecular calculations were carried out by HyperChem [HyperChem 7.51 Version, Hypercube Inc., Florida, USA, 2003]. The molecular geometry of the ligand and its Fe(III) and Cu(II) complexes is first optimized at molecular mechanics (MM)

level. Semi-empirical method PM3 is then used for optimizing the full geometry of the system using Polak–Ribiere (conjugate gradient) algorithm and Unrestricted Hartee–Fock (UHF) is employed keeping RMS gradient of $0.01 \text{ kcal}/\text{\AA mol}$.

2.4. Procedure for the pH-metric titration

The pH-metric measurements were carried out with Hanna Instrument 8519 digital pH meter. All titration were preformed at room temperature. The experimental procedure involves the pH-metric titration of the following solutions against standardized free carbonate sodium hydroxide solution ($1 \times 10^{-3} \text{ mol dm}^{-3}$) and 20% (v/v) ethanol–water solution at constant ionic strength (1 mol dm^{-3}).

- *Solution a*: 2.5 ml HCl (0.01 mol dm^{-3}) + 1 ml KCl (1 mol dm^{-3}) + 5 ml ethanol.
- *Solution b*: 2.5 ml HCl ($0.012 \text{ mol dm}^{-3}$) + 1 ml KCl (1 mol dm^{-3}) + 5 ml ethanol + 5 ml HL ($0.002 \text{ mol dm}^{-3}$).
- *Solution c*: solution b + 5 ml ($0.001 \text{ mol dm}^{-3}$) metal ions.

The above solutions were completed to 25 ml with redistilled water. The \bar{n}_A is calculated applying Irving and Rossotti equations [14]:

$$n_A = Y + \frac{(V_1 - V_2)([A] + [B])}{(V_0 + V_2)T_L}$$

where Y is the ionizable proton(s) of the ligand, V_1 and V_2 are the volumes of alkali required to reach the same pH in HCl and in the ligand curves, respectively, V_0 is the initial volume of the mixture, T_L is the ligand concentration in the initial volume, $[A]$ and $[B]$ are the concentrations of HCl and NaOH, respectively. The n^- and pL values were evaluated by:

$$\bar{n} = \frac{(V_3 - V_2)([A] + [B])}{(V_0 + V_2)\bar{n}_A T_M} \quad (1)$$

$$\text{pL} = \log \frac{1 + K_1[\text{H}^+] + K_1 K_2 [\text{H}^+]^2 + K_1 K_2 K_3 [\text{H}^+]^3}{T_L - \bar{n} T_M} \cdot \frac{V_3 + V_0}{V_0} \quad (2)$$

where V_3 is the volume of alkali required to reach the desired pH in the complex solution and T_M is the initial concentration of the metal ion.

3. Results and discussion

The ability of 3-methyl-5-oxo-N,1-diphenyl-4,5-dihydro-1H-pyrazole-4-carbothioamide to form bimetallic complexes with Co(II), Ni(II), Cu(II) ions and monometallic with Cr(III) and Fe(III) is mainly related to the existence of numerous coordination groups. The isolated metal complexes have been investigated by physical and spectroscopic studies. Stoichiometric ratios of the complexes are 2:3 or 1:3 (M:L) and the compositions are shown in Table 1. Most solids are insoluble in common organic solvents and soluble in DMF and DMSO. All complexes have melting points in the range 185 – 259°C . The steric hindrance due to the large size of the ligand molecule may give lower stability and decreases the melting.

3.1. pH-metric studies

The proton–ligand formation constant and the formation constants of its metal complexes have been determined [15,16]. The values of the average number of protons (n_A), the average number of ligand molecules attached per metal ion (n) and the free ligand exponent (pL) were calculated at different pH values. Plotting of \bar{n}_A versus pH gave the proton–ligand formation curve which is suitable

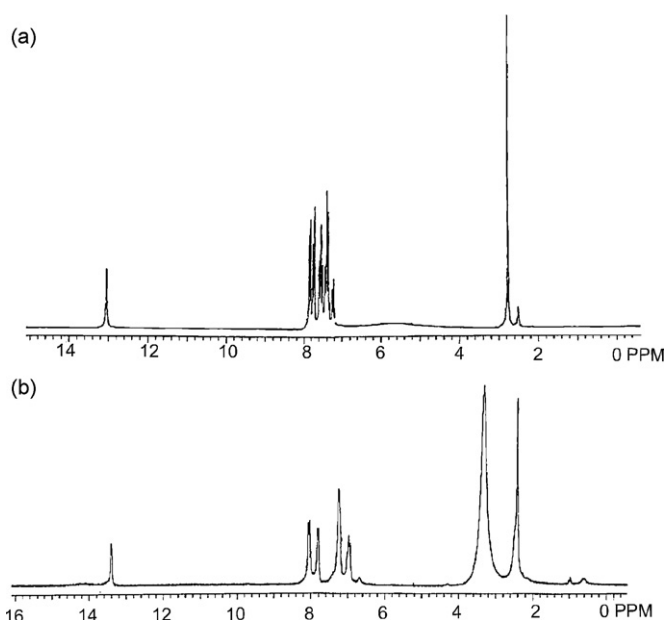


Fig. 2. ^1H NMR spectra of (a) ligand and (b) $[\text{Ni}_2(\text{L})_3(\text{OAc})]$.

Table 1
Elemental analyses and formula weights of the ligand and its metal complexes.

Compound, formula, F.W.	Color	m.p. (°C)	%Found (Calcd.)			
			C	H	N	M
HL, C ₁₇ H ₁₅ N ₃ O ₅ , 309.396	Yellow	193	65.2 (66.0)	4.9 (4.9)	13.4 (13.6)	–
[Cu ₂ (L) ₃ (OAc)], C ₅₃ H ₄₅ N ₉ O ₅ S ₃ , 1111.31	Green	202	57.9 (57.3)	4.1 (4.1)	11.9 (11.4)	11.6 (11.4)
[Co ₂ (L) ₃ (OAc)(H ₂ O) ₄], C ₅₃ H ₅₃ N ₉ O ₉ S ₃ , 1174.15	Brown	185	55.0 (54.2)	4.8 (4.5)	10.6 (10.7)	9.9 (10.0)
[Ni ₂ (L) ₃ (OAc)], C ₅₃ H ₄₅ N ₉ O ₅ S ₃ , 1101.65	Brown	259	57.9 (57.8)	4.7 (4.1)	11.6 (11.4)	10.9 (10.7)
[Cr(L) ₃ (H ₂ O) ₃], C ₅₁ H ₄₈ N ₉ O ₆ S ₃ , 1031.21	Green	186	59.7 (59.4)	4.0 (4.7)	11.7 (12.2)	5.8 (5.3)
[Fe(L) ₃], C ₅₁ H ₄₂ N ₉ O ₃ S ₃ , 981.01	Dark brown	211	61.2 (62.4)	4.6 (4.3)	13.1 (12.9)	5.1 (5.7)

Table 2
Assignments of the IR spectral bands of the ligands and their complexes.

Compound	ν OH	ν NH	ν CH	ν C=O	ν C=N	ν C=N*	δ OH	ν C=S	ν C-S	ν M-O	ν M-S
HL	–	3126	3022	1641	1591	–	–	790	–	–	–
[Cu ₂ (L) ₃ (OAc)]	3413	–	–	–	1594	1562	1391	–	616	455 (s)	375
[Co ₂ (L) ₃ (OAc)(H ₂ O) ₄]	3408	–	–	–	1593	1563	1394	–	615	490, 435	375
[Ni ₂ (L) ₃ (OAc)]	3388	–	–	–	1593	1555	1390	–	625	490, 425	350
[Cr(L) ₃ (H ₂ O) ₃]	–	3130	–	–	1595	1553	1393	790	–	470, 390	–
[Fe(L) ₃]	3406	–	–	–	1594	1549	1393	–	620	460	340

for the calculation of the ligand constant ($\log K_1$); the value (5.04) is due to thione proton. The stability constants of the complexes have been calculated by half method. The data reveal that Cr(III), Fe(III) and Co(II) gave 1:1, 1:2 and 1:3 ratios while Cu(II) gave 1:2 and 1:3. The overall stability constants of the complexes reveal the following order:

$$\text{Fe (11.75)} > \text{Cr (11.7)} > \text{Co (11.45)} > \text{Cu (7.07)}$$

3.2. IR spectra

The IR bands of the coordination sites of the ligand (Table 2) showed that it may coordinates through the hydroxyl and thiol group in all complexes except [Cr(L)₃(H₂O)₃] in which the ligand acts as a monodentate through the enolized carbonyl atom. The following remarks may support this behavior:

- The disappearance of the bands due to ν (NH), ν (CH), ν (C=O) and ν (C=S) with the appearance of ν (OH), ν (C=N*), δ (OH) and ν (C-S) at 3388–3408, 1549–1563, 1390–1394 and 616–625 cm⁻¹ indicating the formation of C–OH and C–SH with liberating the SH proton. In [Cr(L)₃(H₂O)₃], the spectrum showed the disappearance of ν (CH) and ν (C=O). The ν (NH) and ν (C=S) bands are observed at 3130 and 790 cm⁻¹ similar to those observed in the ligand spectrum.
- The appearance of ν (OH) strong is due to the enolization of the CH proton adjacent to the carbonyl group with the existence of the OH protonated. The appearance of δ (OH) is a further support for the enolization.
- The appearance of ν (M–O) and ν (M–S) at 450–470 and 340–390 cm⁻¹ [17] indicates the chelation through oxygen and sulfur atoms.

Table 3
Magnetic moments and electronic spectral bands of the complexes.

Complex	μ_{eff} (BM)	State	d–d transition (cm ⁻¹)	Ligand and charge transfer transitions (cm ⁻¹)	Supposed structure
HL	–	DMF		37,315; 32,260; 27,930; 26,180	
[Cu ₂ (L) ₃ (OAc)]	1.28	DMF	20,000; 17,575; 15,850; 14,180	24,000; 22,560; 21,280	Square-planar
[Co ₂ (L) ₃ (OAc)(H ₂ O) ₄]	1.92	DMF	18,940; 18,100; 16,950; 16,300	25,000; 21,960; 20,660	Low spin octahedral
[Ni ₂ (L) ₃ (OAc)]	0.00	DMF	20,240; 18,380; 17,570; 17,000; 14,500	22,220; 21,000	Square-planar
[Cr(L) ₃ (H ₂ O) ₃]	4.22	DMF	24,500, 15,870	37,310; 32,260; 27,930	Octahedral
[Fe(L) ₃]	6.18	DMF	20,100; 18,140; 16,950; 16,470	22,200	Octahedral

- The appearance of two bands at 530 and 490 cm⁻¹ in the spectrum of [Cr(L)₃(H₂O)₃] is due to ν (M–OH₂) and ν (M–O), respectively.
- The two bands at 1507–1496 and 1429–1426 cm⁻¹ in the Co(II), Ni(II) and Cu(II) complexes with difference ca. 75 cm⁻¹ may support the bidentate nature of the acetate group [18].
- The broad bands at ~3408, ~1650, ~840, ~590 cm⁻¹ in [Co₂(L)₃(OAc)(H₂O)₄] and [Cr(L)₃(H₂O)₃] are attributed to the ν (OH), δ (H₂O), ρ_r (H₂O) and ρ_w (H₂O) vibrations of the coordinated water [19].

3.3. Magnetic and spectral studies

The magnetic moments and the electronic spectral bands of the studied metal complexes are given in Table 3. [Cr(L)₃(H₂O)₃] and [Fe(L)₃] have magnetic moments of 4.22 and 6.18 BM in the range reported for the existence of three and five unpaired electrons. The Co(III) and Cu(II) complexes measured subnormal values than that reported for three and one unpaired electrons. The value measured for the Co(II) complex (1.92 BM) may indicate low spin octahedral or a square-planar geometry while the value measured for the Cu(II) complex (1.28 BM) indicates Cu···Cu interaction. The zero moment for the Ni(II) complex indicates it is a square-planar structure.

The solution electronic spectra of the ligand and its complexes were included in Table 3. The bands recorded at 37,315, 32,260, 27,930 and 26,180 cm⁻¹ in the ligand spectrum may be due to the $\pi \rightarrow \pi^*$ and $n \rightarrow \pi^*$ transitions of NHC=S and C=N groups [20]. These bands are shifted in the spectra of all complexes to lower wavenumbers while the other bands to some extent changed or disappeared. The band at 22,000–26,000 cm⁻¹ in the spectra of complexes may be due to LMCT.

The electronic spectrum of [Cr(L)₃(H₂O)₃] in DMF solution showed two broad absorption bands centered at 15,870 (ν_2)

Table 4
Decomposition steps and removing species of the complexes.

Complex	Temperature range (°C)	Species removed	Found (Calcd.), %
[Cu ₂ (L) ₃ (OAc)]	166–265	–(OAc + 3PhN + Ph)	36.2 (36.8)
	266–334	–(2Ph + 3Me + 2C ₄ H ₉ N ₂ O)	35.4 (34.7)
	335–604	–C ₄ H ₉ N ₂ O	8.0 (8.4)
	605–750	–2CuS + S	20.3 (20.0)
[Co(L) ₃ (OAc)(H ₂ O) ₄]	185–254	–(4H ₂ O + OAc + 3Me + PhN)	23.0 (22.8)
	271–366	–(PhN + Ph + C ₄ H ₉ N ₂ O)	24.2 (22.3)
	367–465	–PhN	8.9 (7.8)
	466–616	2Ph + C ₅ H ₂ N ₄ O	25.2 (25.9)
	617–750	2CoS + S + 3C	20.2 (21.3)
[Ni ₂ (L) ₃ (OAc)]	225–267	–OAc + PhN + Ph + 3Me	24.6 (24.7)
	268–300	–2PhN + Ph + C ₄ H ₉ N ₂ O	32.0 (31.9)
	301–514	–Ph + 3C	10.0 (10.2)
	515–564	–C ₂ H ₂ N ₄ O ₂	9.7 (10.4)
	565–800	–2NiS + S + 3C	23.7 (22.7)
[Fe(L) ₃]	179–259	–2Ph	15.3 (15.7)
	260–343	–2Ph	14.6 (15.7)
	344–479	–2Ph + 3Me + N ₃	25.7 (24.6)
	480–619	–C ₃ H ₃ N ₆ O ₃	18.0 (17.4)
[Cr(L) ₃ (H ₂ O) ₃]	620–750	–FeS + 2S + 9C	25.0 (26.5)
	240–288	–3H ₂ O	5.9 (5.2)
	289–356	–2PhN	17.2 (17.7)
	357–420	–PhN + 3Me	12.6 (13.2)
	421–467	–2Ph + 3C	19.0 (18.4)
	468–533	–Ph + C ₉ H ₃ N ₆ O ₃	31.1 (31.3)
544–700	–CrS + 2S	14.2 (14.4)	

and 24,500 (ν_3) cm^{-1} attributed to the ${}^4A_{2g} \rightarrow {}^4T_{1g}$ (P) (ν_2) and ${}^4A_{2g} \rightarrow {}^4T_{2g}$ (F) (ν_3) transitions in an octahedral geometry. The ligand field parameters ($Dq = 750 \text{ cm}^{-1}$, $B = 790 \text{ cm}^{-1}$ and $\beta = 0.86$) support the proposed geometry.

The electronic spectrum of the Cu(II) complex showed four bands in the range 14,180–20,000 cm^{-1} . The band at 20,000 cm^{-1} is corresponding to the ${}^2B_{1g} \rightarrow {}^2E_g$ transition in a square-planar geometry [21]. The presence of the other bands may be due to the distortion of the planar geometry due to Cu...Cu interaction or to the presence of S and O sites having different polarities (Fig. 3). Its molecular modeling is shown in Fig. 2S.

The electronic spectrum of the Fe(III) complex showed three bands at 22,200, 21,100 and 18,140 cm^{-1} due to the ${}^6A_{1g} \rightarrow {}^4T_{1g}$, ${}^6A_{1g} \rightarrow {}^4T_{2g}$ and ${}^6A_{1g} \rightarrow {}^4T_{1g}$ transitions in a high spin octahedral geometry [22]. Its structure is shown in Fig. 4 and its molecular modeling is drawn as in Fig. 3S. The HOMO and LUMO values are –8.288 and –1.632 eV.

The magnetic moment value of the Co(II) complex (1.92 BM) indicate a low spin octahedral or a square-planar geometry. In its electronic spectrum, the bands at 18,940, 16,300, 21,960 and 25,000 cm^{-1} are assignable to the d–d and charge transfer transitions. The first two bands suggest a low spin octahedral structure rather than a square-planar [23].

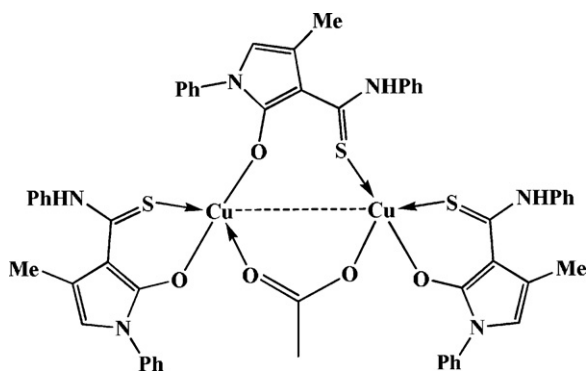


Fig. 3. Structure of Cu(II) complex.

In the spectrum of Ni(II) complex, the bands at 22,220, 21,000, 20,240, 18,380, 17,570, 17,000 and 14,500 cm^{-1} are assignable to charge transfer and d–d transitions. The bands at 20,240 and 18,380 cm^{-1} may be due to the ${}^2B_{2g} \rightarrow {}^2A_{1g}$ and ${}^1A_{1g} \rightarrow {}^2A_{2g}$ transitions in a square-planar structure [24]. Further support for the square-planar configuration comes from its ${}^1\text{H}$ NMR spectrum (Fig. 2b) which is recorded and compared with that of the ligand. A fruitful observation is the appearance of a peak due to the CH_3 group of acetate at 3.343 ppm.

3.4. ESR spectrum of the Cu(II) complex

The spin Hamiltonian parameters and the G value of the solid-state [Cu₂(L)₃(OAc)] are calculated. Its ESR spectrum displayed axially symmetric g -tensor parameters indicating the ground state is $dx^2 - y^2$. The value of $G = (g_{\parallel} - 2)/(g_{\perp} - 2)$ is 2.3 indicating a considerable exchange interaction [25]. The spectrum (Fig. 5) showed g_{\parallel} (2.14) $>$ g_{\perp} (2.06) $>$ 2.0023. This observation with a weak ESR absorption band at 14,140 G is consistent with a square-planar geometry [26,27]. A forbidden magnetic dipolar transition is also observed at half-field (ca. 1600 G, $g \approx 4.0$), but the intensity is very weak. The present ESR spectrum is similar to the ESR spectra of

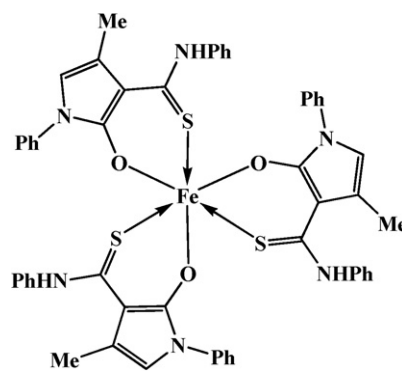


Fig. 4. Structure of Fe(III) complex.

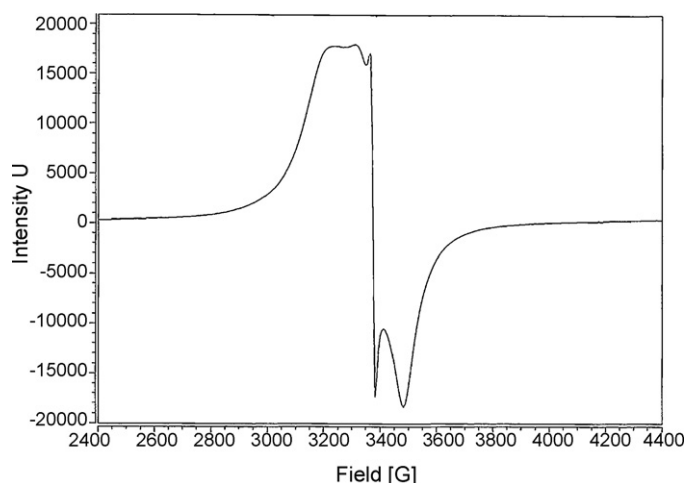


Fig. 5. ESR spectrum of $[\text{Cu}_2(\text{L})_3(\text{OAc})]$.

the binuclear Cu(II) complexes [28]. The appearance of the half-field signal confirms that the complex has a binuclear unit and that there exists a magnetic interaction between the two Cu(II) ions.

The spectrum (Fig. 4) exhibits broad single line, nearly isotropic signal centered at $g=2.06$ which is attributable to dipolar broadening and enhanced spin lattice relaxation [29]. The line broadening is probably due to insufficient spin-exchange narrowing toward the coalescence of four copper hyperfine lines to a single line. Note that, the same kind of powder ESR line shape has also been observed for many square-planar dimeric Cu(II) complexes with a considerably strong intradimeric spin-exchange interaction.

The $g_{\parallel}/A_{\parallel}$ ratio measured from the ESR spectrum may be considered as an empirical index for tetrahedral distortion; values lower than 135 cm have been observed for square-planar structures. The value measured here is 142.6 cm is closed to those observed for distorted complexes.

Molecular orbital coefficients, α^2 and β^2 , were calculated using the following equations [30]:

$$A_{\parallel} = -PK - \frac{4\beta^2 p}{7} - (g_e - g_{\parallel})P - \frac{3}{7}(g_e - g_{\perp})P$$

$$A_{\perp} = -PK + \frac{2\beta^2 p}{7} - \frac{11}{14}(g_e - g_{\perp})P$$

$$g_0 - g_{\parallel} = \frac{8\alpha^2 \beta^2 \lambda}{E}$$

where $P=136$ G (the dipolar interaction constant between magnetic moment of the electron and vanadium nucleus), $\lambda=170$ cm^{-1} and E is the d-d band and k is the Fermi contact term. The value of β^2 is much lower than α^2 . The β^2 (0.57) compared to α^2 (0.64) indicates that the in-plane π bonding is more covalent than the in-plane σ -bonding. Its molecular modeling shown in Fig. 5 has the HOMO and LUMO energies -7.699 and -2.452 eV, respectively. The Cu-Cu distance is calculated to be 3.772 Å.

3.5. Thermal analysis

The stages of decomposition, temperature range, decomposition product as well as the found and calculated weight loss percentages of the complexes are given in Table 4.

The TGA curves of $[\text{Co}(\text{L})_2(\text{OAc})(\text{H}_2\text{O})_4]$ and $[\text{Ni}(\text{L})_2(\text{OAc})]$ are similar and showed the first decomposition step beginning at 185 and 225 °C, respectively. The lower temperature in case of Co(II) is due to the elimination of 4H₂O. A plateau obtained at 600–800 °C is referring to 2MS + 3C + S as a residual part.

The TG curves of $[\text{Cr}(\text{L})_3(\text{H}_2\text{O})_3]$ and $[\text{Fe}(\text{L})_3]$ were compared. The first step in $[\text{Cr}(\text{L})_3(\text{H}_2\text{O})_3]$ with weight loss of 5.9 (Calcd. 5.2%)

at 240–288 °C is corresponding to the removal of the coordinated water. The step in $[\text{Fe}(\text{L})_3]$ (179–259 °C) represents the beginning of the complex decomposition. The residue at 800 °C in Cr(III) complex was CrS + 2S while in the Fe(III) complex was FeS + 2S + 9C.

3.6. Kinetic data

The expression for the thermal decomposition of a homogeneous system has the following general form:

$$\frac{d\alpha}{dt} = K(T)g(\alpha) \quad (3)$$

where α represent the reaction extent of the component of the sample being degraded, defined by:

$$\alpha = \frac{w_0 - w_t}{w_0 - w_{\infty}} \quad (4)$$

w_0 , w_t and w_{∞} are the weights of the sample before the degradation, at temperature t and after total conversion, respectively. $K(T)$ is the rate coefficient that usually follows the Arrhenius equation. The differential conversion function, $g(\alpha)$ may present various functional forms but its most commonly form for solid-state reactions is $g(\alpha)=(1-\alpha)^n$, where n is the reaction order, assumed to remain constant during the reaction [31,32]. At a certain heating rate $\beta=dT/dt$, we have:

$$\frac{d\alpha}{(1-\alpha)^n} = \frac{A}{\beta} \exp\left(-\frac{E}{RT}\right) dT \quad (5)$$

where E and A are the activation energy and the Arrhenius pre-exponential factor, respectively. A number of pyrolysis processes can be represented as a first order reaction. Particularly, the degradation of a series of H₃EPTS complexes was suggested to be first order, therefore we assume $n=1$ for the remainder of the present text. Under this assumption, the integration of Eq. (5) leads to:

$$\ln(1-\alpha) = -\frac{A}{\beta} \int_{T_0}^T \exp\left(-\frac{E}{RT}\right) dT \quad (6)$$

Several approximations for evaluation of the thermo kinetic parameters A and E from a single thermogravimetric experiment were carried out at a given heating rate. Two methods that differ on the way of resolving Eq. (6) are compared using the TGA data of the studied complexes. The Coats-Redfern [33] relation is as follows:

$$\ln\left[-\frac{\ln(1-\alpha)}{T^2}\right] = \ln\left(\frac{AR}{\beta E}\right) - \frac{E}{RT} \quad (7)$$

A plot of $\ln[-(\ln(1-\alpha))/T^2]$ versus $1/T$ gives a straight line whose slope (E/R) and the pre-exponential factor (A) can be determined from the intercept.

The Horowitz-Metzger relation is as follows:

$$\ln[-\ln(1-\alpha)] = \frac{E\theta}{RT_s^2} \quad (8)$$

where $\theta=T-T_s$, T_s is the DTG peak temperature, T is the temperature corresponding to weight loss w_t . A straight line should be observed between $\ln[-\ln(1-\alpha)]$ and θ with a slope of E/RT_s^2 . The other thermodynamic parameters can be calculated by [34]:

$$\Delta H = E - RT; \quad \Delta S = R \ln \frac{hA}{k_B T}; \quad \Delta G = \Delta H - T\Delta S \quad (9-11)$$

In order to assess the influence of the structural properties of the ligand and the type of the metal on the thermal behavior of the complexes, n and E of the various decomposition stages were determined using the Coats-Redfern [33] and Horowitz-Metzger [35] methods (Table 5). In both methods, the left side of Eqs. (7) and (8) are plotted against $1000/T$ and θ , respectively (Fig. 5). From the results, the high values of the energy of activation reveal high

Table 5
Kinetic and thermodynamic parameters of the thermal decomposition of Fe(III) and Cr(III) complexes.

Compound	Step (°C)	Coats–Redfern eqn.			Horowitz–Metzger eqn.			ΔS^*	ΔH^*	ΔG^*
		<i>R</i>	<i>n</i>	<i>E</i>	<i>r</i>	<i>n</i>	<i>E</i>			
[Fe(L) ₃]	1st 493	0.9972	0.00	79.9	0.9966	0.00	89.10	–180.00	75.80	164.50
		0.9988	0.33	89.9	0.9983	0.33	98.90	–158.00	85.50	163.40
		0.9997	0.66	100.4	0.9994	0.66	109.80	–134.10	96.30	16.40
		<u>1.000</u>	1.00	11.25	0.9999	1.00	122.3	–113.90	108.40	164.50
		0.9978	2.00	154.30	0.9988	2.00	164.9	–15.90	150.20	158.00
		0.9857	0.00	72.50	0.8959	0.00	82.60	–224.60	66.80	221.30
	3rd 688	0.9912	0.33	83.40	0.9906	0.33	93.60	–228.40	77.70	234.80
		0.9952	0.66	95.40	0.9941	0.66	105.70	–210.00	89.70	234.20
		0.9977	1.00	109.30	0.9967	1.00	119.40	–212.90	103.60	250.10
		<u>0.9988</u>	2.00	158.10	0.9992	2.00	168.00	–110.10	152.40	228.10
		0.9684	0.00	89.20	0.9712	0.00	97.10	–195.90	84.30	200.30
		0.9763	0.33	104.00	0.9777	0.33	111.30	–167.80	99.10	198.40
[Cr(L) ₃ (H ₂ O) ₃]	2nd 592	0.9880	0.66	120.30	0.9832	0.66	127.30	–139.80	115.40	198.20
		0.9881	1.00	138.80	0.9877	1.00	145.60	–130.90	133.90	211.4
		<u>0.9968</u>	2.00	205.70	0.9960	2.00	211.40	21.6	200.80	188.00
		0.9684	0.00	89.20	0.9712	0.00	97.10	–195.90	84.30	200.30

E, ΔH^* and ΔG^* are in kJ mol^{–1}, ΔS^* in J mol^{–1}; the underlined values of *r* represent the best fit values.

stability of such chelates due to their covalent bond character [36]. The positive sign of ΔG for the different decomposition steps indicates that the free energy of the final residue is higher than that of the initial compound, and hence all decomposition steps are non-spontaneous processes. The negative ΔS values are due to the high value of mid point temperature of the decomposition step (*T*) and the low value of pre-exponential factor (*A*). Applying Eq. (10) for *T* and *A*, negative values were obtained indicating more ordered for the activated complex than the reactants or the reaction is slow [37].

Appendix A. Supplementary data

Supplementary data associated with this article can be found, in the online version, at doi:10.1016/j.saa.2009.06.015.

References

- [1] G.H. Van Giessen, J.A. Crim, D.H. Petering, J. Natl. Cancer Inst. 51 (1973) 139.
- [2] V. Sharma, V. Sharma, R. Bohra, J.E. Drake, M.B. Hursthouse, M.E. Light, Inorg. Chim. Acta 360 (2007) 2009.
- [3] (a) A.A. Abou-Hussen, A.A. Emara, Coord. Chem. 57 (2004) 973; (b) R.M. El-Shazly, G.A.A. Al-Hazmi, S.E. Ghazy, M.S. El-Shahawi, A.A. El-Asmy, Coord. Chem. 59 (8) (2006) 846.
- [4] H. Stunzi, Aust. J. Chem. 35 (1982) 1145.
- [5] N.M. El-Metwally, G.A. Al-Hazmi, A.A. El-Asmy, Transit. Metal Chem. 31 (2006) 673.
- [6] I.M. Saad, M.S. El-Shahawi, H. Saleh, A.A. El-Asmy, Transit. Metal Chem. 32 (2) (2007) 156.
- [7] N.M. El-Metwally, R.M. El-Shazly, E. Gabr, A.A. El-Asmy, Spectrochim. Acta 61A (2005) 1113.
- [8] D.X. West, A.E. Libertia, S.B. Pandhey, Coord. Chem. Rev. 123 (1993) 49.
- [9] D.C. Dash, A.K. Panda, A. Mahapatra, S.B. Patjoshi, J. Indian Chem. Soc. 79 (2002) 642.
- [10] R.M. El-Shazly, Transit. Metal Chem. 25 (2000) 183.
- [11] R.M. El-Shazly, Transit. Metal Chem. 16 (1991) 492.
- [12] R.M. El-Shazly, Chem. Pharm. Bull. 47 (1999) 1614.
- [13] M.A. Metwally, E. Abdel-Latif, F.A. Amer, Boll. Chim. Farmac.-Anno 139 (2000) 213.
- [14] H.M. Irving, H.S. Rossotti, J. Chem. Soc. (1954) 2904.
- [15] J.L. Mesa, J.L. Pizarro, M.I. Arriortua, Cryst. Res. Technol. 33 (1998) 489.
- [16] V.T. Kasumo, Spectrochim. Acta A 57 (2001) 1649.
- [17] P. Souza, F. Kaiser, J.R. Mogueer, A. Arquerro, Transit. Metal Chem. 12 (1987) 128.
- [18] R.M. El-Shazly, G.A.A. Al-Hazmi, S.E. Ghazy, M.S. El-Shahawi, A.A. El-Asmy, Spectrochim. Acta A 61 (2005) 243.
- [19] A.A. El-Asmy, M.A. Hafez, E.M. Saad, F.T. Taha, Transit. Metal Chem. 19 (1994) 603.
- [20] G.A.A. Al-Hazmi, M.S. El-Shahawi, I.M. Gabr, A.A. El-Asmy, J. Coord. Chem. 58 (8) (2005) 713.
- [21] A.A. El-Asmy, G.A.A. Al-Hazmi, Spectrochim. Acta 71A (2009) 1885.
- [22] O.A. Al-Gammal, A.A. El-Asmy, J. Coord. Chem. 61 (14) (2008) 2296.
- [23] A.A. El-Asmy, K.M. Ibrahim, M.M. Bekheit, M.M. Mostafa, Synth. React. Inorg. Met.-Org. Chem. 15 (3) (1985) 287.
- [24] N.M. El-Metwally, A.A. Abou-Hussen, A.A. El-Asmy, IJPAC 1 (2006) 75.
- [25] B.J. Hathaway, Struct. Bond. (Berlin) 57 (1984) 55.
- [26] M.L. Miller, S.A. Ibrahim, M.L. Golden, M.Y. Daresbourny, Inorg. Chem. 42 (1998) 2999.
- [27] A. Diaz, A. Fragosa, R. Cao, V. Verej, J. Carbohydr. Chem. 17 (1998) 293.
- [28] O. Khan, T. Mallah, J. Gouteron, S. Jeanin, Y. Jeanin, J. Chem. Soc., Dalton Trans. (1989) 1117.
- [29] (a) B.J. Hathaway, D.E. Billing, Coord. Chem. Rev. 5 (1970) 143; (b) H. Yokoi, M. Chikira, J. Am. Chem. Soc. 97 (1975) 3975; (c) V.H. Growford, W.E. Hatfield, Inorg. Chem. 16 (1977) 1336.
- [30] A.A. El-Asmy, I.M. Gabr, N.M. El-Metwally, S.E. Ghazy, D.A. Abdel-Basseer, Coord. Chem. 61 (22) (2008) 3620.
- [31] T. Taakeyama, F.X. Quinn, Thermal Analysis Fundamentals and Applications to Polymer Science, John Wiley and Sons, Chichester, 1994.
- [32] J.F. Mano, D. Koniarova, R.L. Reis, J. Mater. Sci.: Mater. Med. 14 (2003) 127.
- [33] A.W. Coats, J.P. Redfern, Nature 20 (1964) 68.
- [34] A. Broido, J. Polym. Sci. 7 (1969) 1761.
- [35] H.H. Horowitz, G. Metzger, Anal. Chem. 25 (1963) 1464.
- [36] R.G. Mortimer, Physical Chemistry: A. Harcourt and Science Technology Company, Academic Press, San Diego, 2000.
- [37] A.A. Frost, R.G. Pearson, Kinetics and Mechanisms, Wiley, New York, 1961.